CREATED USING THE RSC LaTeX PCCP ARTICLE TEMPLATE – SEE www.rsc.org/electronicfiles FOR DETAILS

Structural band-gap tuning in g-C_3N_4

Sebastian Zuluaga,[a] Li-Hong Liu,[b] Natis Shafiq,[b] Sara Rupich,[b] Jean-François Veyan,[b] Yves J. Chabal,[b] and Timo Thonhauser*[a]

Received Xth XXXXXXXXXX 20XX, Accepted Xth XXXXXXXXX 20XX
First published on the web Xth XXXXXXXXXX 200X
DOI: 10.1039/b000000x

arXiv:1412.3485v1 [cond-mat.mtrl-sci] 10 Dec 2014

g-C_3N_4 is a promising material for hydrogen production from water via photo-catalysis, if we can tune its band gap to desirable levels. Using a combined experimental and *ab initio* approach, we uncover an almost perfectly linear relationship between the band gap and structural aspects of g-C_3N_4, which we show to originate in a changing overlap of wave functions associated with the lattice constants. This changing overlap, in turn, causes the unoccupied p_z states to experience a significantly larger energy shift than any other occupied state (s, p_x, or p_y), resulting in this peculiar relationship. Our results explain and demonstrate the possibility to tune the band gap by structural means, and thus the frequency at which g-C_3N_4 absorbs light.

1 Introduction

Hydrogen production is a critical step in a possible future hydrogen economy.[1–4] Water, due to its abundance, could be an ideal source of hydrogen in the production process. Among the various ways to split water, photocatalysis—using the sun as a source of energy and a photocatalytic material—is one of the most promising methods.[5–14] However, the use of sunlight sets two important restrictions on the photo-catalytic material used as anode: First, it should be a semiconductor capable of absorbing light in the visible range of the solar spectrum (between 1.6 and 3.2 eV). Second, the H^+/H_2 and the O_2/H_2O electrode potentials should lie in-between the edges of the conduction and valence bands. One of the most studied semiconductors for this purpose is TiO_2,[15–25] however, its large band gap of 3.2 eV restricts adsorption to the UV range of the spectrum.[5] Thus, the search for better suited materials is a highly active field of current research.

Graphitic carbon nitride g-C_3N_4 is a layered system well known for having a band gap of 2.7 eV.[26] It is the most stable allotrope of carbon nitrides at ambient condition,[27] consisting of abundant elements. It is an efficient visible light photocatalytic material,[28–30] which exhibits promising properties towards the reduction of CO_2 and other pollutants.[31–35] In addition, g-C_3N_4 has shown remarkable properties toward the photocatalytic splitting of water.[36,37] Also, the edges of the conduction and valence bands are in the correct position with respect to the H^+/H_2 reduction and O_2/H_2O oxidation potentials. X-ray diffraction (XRD) shows that the distance between layers is ∼3.26 Å, while the in-plane lattice constant varies from 6.71 to 6.81 Å.[38,39] Although the band gap is only slightly above its optimal value, the photo-catalytic activity could significantly benefit from a small band-gap reduction. To this end, g-C_3N_4 has been doped with S,[40,41] B,[30] P,[42] C,[43] O,[44] Zn,[45] and B–F.[46] Unfortunately, most dopants do not show the desired effect; they increase the band gap, leave it unaffected, or turn the system metallic. Among those dopants, the most promising is O. Li and co-workers[44] found that the O-doped g-C_3N_4 has a band gap of 2.49 eV and consequently exhibits a better visible-light photo-activity. Using X-ray photoelectron spectroscopy (XPS), Raman, and Fourier transform infrared spectroscopy analysis, the authors were able to determine that the introduced O atoms replace N atoms and their XRD measurements showed that the peak located at 27.3° shifted to 27.5°, indicating that the layer distance decreased from 3.26 Å to 3.24 Å. While this is significant progress, O doping by itself does not allow to tune the band gap to any desired level. Furthermore, a clear understanding of what influences the band gap in a predictive way is still lacking. Motivated by the influence of O doping on the layer separation, we pursue here a different route and explore the relationship between the band gap and purely structural aspects of g-C_3N_4.

In 2009, Wang et al.[38] found an interesting—but as of yet unexplained—correlation between the temperature at which their g-C_3N_4 samples were prepared and the band gap: An increase in the temperature results in a decrease in the band gap. In the same work, the authors also report a change in the XRD peak located at 27.3° towards higher angles as the temperature increases. Similar results were found by Dong and co-workers.[28] This experimental evidence strongly suggests a direct relationship between the layer separation and the band gap in g-C_3N_4, but this relationship was not explored in either of those works, as the focused was on sample preparation and characterization. The investigation of this relationship and its

[a] *Department of Physics, Wake Forest University, Winston-Salem, North Carolina 27109, USA; E-mail: thonhauser@wfu.edu*
[b] *Department of Materials Science and Engineering, University of Texas at Dallas, Dallas, Texas 75080, USA*

underlying physics is the main focus of the present article.

It is well known that several systems exhibit a relationship between structural aspects and the band gap.[47–50] Of particular interest is the similarly-layered graphene monoxide, where the band gap can be tuned through strain.[51] In this case, the change of the band gap was shown to be due to large variations in the conduction band, while the valence band experiences only small changes upon deformation of the system's geometry. This particular finding guided our own research on g-C_3N_4.

2 Experimental and Computational Details

2.1 Experimental Details

In a typical synthesis, 2 g of melamine monomer (TCI) were put into an alumina boat with a cover, and heated to a certain temperature in the range of 500 – 650 °C with a ramp rate of 5 °C·min^{-1} in a horizontal tube furnace (Carbolite MTF3216) under flowing Ar, and then the temperature was kept at the certain temperature (500, 550, 600, or 650 °C) for 4 hours. The resulting powders with color from light yellow to light brown—see the inset in the lower panel of Figure 1—were collected for use without further treatment. This change in color has been observed by other groups and is believe to be due to the change in the layer condensation and the change in the band gap of the system.[37]

XRD diffraction patterns were recorded for 2θ values ranging from 5° to 60° in order. X-ray diffraction measurements were conducted with a Rigaku Ultima III diffractometer (Cu Kα radiation, X-ray wavelength of 1.54187 Å, operating at 40 keV with a cathode current of 44 mA). For visualization purposes, a running average over 20 data points has been made to plot the XRD data. The UV-Vis spectra were obtained for the dry-pressed KBr disk samples using Cary 5000 UV-Vis-NIR spectrophotometer. The spectra were recorded from 200 – 800 nm at ambient conditions.

2.2 Computational Details

Our *ab initio* calculations were performed at the DFT level with the VASP code.[52] We used projector augmented wave (PAW) pseudopotentials[53] and a plane-wave expansion with a kinetic-energy cutoff of 983 eV. Due to the strong van der Waals interaction between the layers of g-C_3N_4, we used the vdW-DF exchange-correlation functional.[54–56] In all cases, we relaxed our systems until the forces on all atoms were less than 1 meV/Å. We used a k-point sampling of $5 \times 5 \times 5$ centered at the Γ point.

To model g-C_3N_4, we constructed a hexagonal supercell with lattice vectors of magnitude $a = b$ and c. The supercell contains two stacked tri-s-triazine units in order to simulate possible stacking configurations. Throughout this manuscript we will refer to the separation between layers as d, which is exactly half the lattice constant c, i.e. $d = c/2$. Each tri-s-triazine unit is comprised of eight N atoms and six C atoms—thus, our systems contain 28 atoms in their supercell.

We used the *GW* approximation at the level of G_0W_0 to calculate the electronic structure of the system and its band gap.[57] The same approach has given excellent agreement with experiments in our previous work on this material.[58] The Green's function and the screened Coulomb interaction were calculated within DFT, where the exchange energy was treated at the level of Hartree Fock. The Green's function and the dielectric matrix were calculated using 140 bands, while the cutoff energy for the response function was set to a value of 90 eV.

3 Results

3.1 Layer Stacking and Band Gap

We begin by reporting the experimental layer separation and band gap. XRD measurements were taken on the four g-C_3N_4 samples prepared at 500, 550, 600, and 650 °C. In addition, the band gap of these samples was measured through the absorbance in the UV-Vis spectrum; results are shown in Figure 1. The upper panel clearly shows the peak at ∼27°, which increases from 27.1° to 27.3° as the temperature increases from 500 to 650 °C, corresponding to a reduction of the interlayer distance d from 3.290 to 3.267 Å. In the lower panel of this figure, the Tauc plot shows that the band gap decreases from 2.75 to 2.62 eV over the same temperature range. Using ultraviolet photoelectron spectroscopy (UPS) we were able to determine that the valence bands of the samples prepared at 500, 550, and 600 °C are located 0.9 eV below the Fermi level, while the valence band of the sample prepared at 650 °C is located 1.13 eV below the Fermi level (see the supplementary materials for further details). As mentioned earlier, the behavior of the layer separation and band gap as a function of sample preparation temperature has been observed separately before,[28,38,44] but a direct relationship between the lattice constant and band gap was not considered.

To explain the above experimental results, further insight into the structure of g-C_3N_4 is needed. Unfortunately, the XRD spectra do not allow for a detailed structural analysis. While the large peak around 27° is related to the layer separation and reveals insightful information, the subtleties of the precise layer stacking is encoded in a series of peaks at higher angles (see Figures S1 and S2 in the supplementary materials), which cannot be resolved experimentally. Note that, in the upper panel of Figure 1 there is another feature around 45°, which we will analyze further below. As such, we will use a combined experimental and theoretical approach to shed

This journal is © The Royal Society of Chemistry [year]

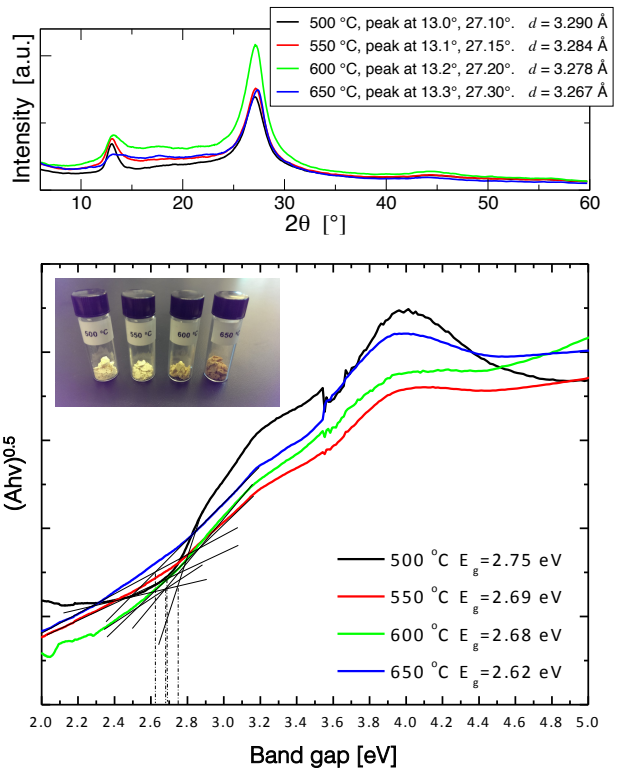

Fig. 1 (top) Experimental XRD pattern of the four g-C_3N_4 samples prepared at 500, 550, 600, and 650 °C. (bottom) $(Ahv)^{1/2}$ vs. photon energy for the same four g-C_3N_4 samples. In the inserted figure the four g-C_3N_4 samples are shown. The corresponding band gaps are shown in the legend.

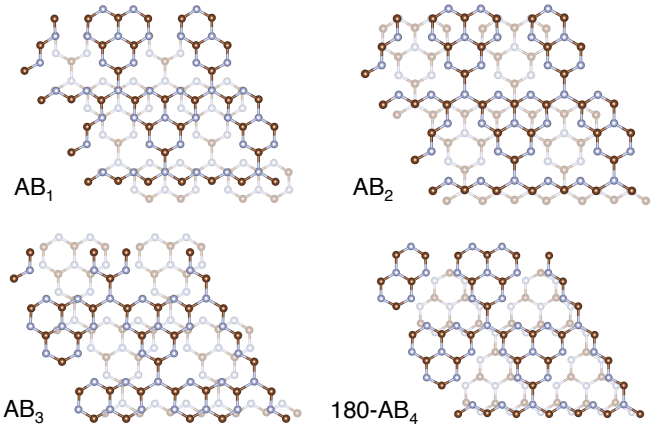

Fig. 2 Layer stackings of g-C_3N_4 considered in this study.

Table 1 Calculated relative energy ΔE in eV per unit cell between different stackings of g-C_3N_4, as well as optimized lattice constants a, b, and $d = c/2$ in Å and band gaps E_g in eV. $a = b$ refers to the in-plane lattice constants, while $d = c/2$ measures the distance between layers.

Stacking	ΔE	$a = b$	d	E_g
AA	0.86	7.174	3.632	3.13
AB_3	0.14	7.177	3.313	3.00
AB_1	0.12	7.178	3.301	2.93
AB_2	0.12	7.177	3.296	2.93
180-AB_4	0.00	7.178	3.297	2.86

light on the layer stacking as a function of temperature.

The layer stacking of g-C_3N_4 exhibits several (meta)stable configurations, located at local minima in the potential energy surface. To find possible stackings, we performed a quasi-random structure search, starting from more than 20 possible different stackings, which were subsequently relaxed. Surprisingly, all starting configurations relax to one of only four possible final stackings, which are depicted in Figure 2. The family of AB stackings (AB_1, AB_2, and AB_3) exhibits tri-*s*-triazine units in adjacent layers that are shifted with respect to each other. The nomenclature 180-AB refers to a situation where the tri-*s*-triazine unit in one layer is rotated 180° with respect to the adjacent layer—in this family we only find one member, which we label 180-AB_4. Interestingly, stacking the tri-*s*-triazine units exactly on top of each other (referred to as AA) is not amongst the local minima; it is very high in energy (see Table 1) and will not be considered further here.

Table 1 shows the lattice constants, relative energy, and band gaps of the different stacking configurations. As expected, the lattice constants a and b are almost not affected by the stacking configuration. Our values of a and b differ slightly from our own XRD measurements and other groups,[38] which indicate $a = 6.81$ Å, however, yet other groups also report $a = 7.3$ Å.[59] On the other hand, our results are in good agreement with the dimensions of the tri-*s*-triazine unit, i.e. $a \simeq 7.13$ Å.[38] Overall, we find the stacking 180-AB_4 to be lowest in energy, band gap, and layer separation, and a direct relationship between those quantities becomes apparent.

We combine our experimental and theoretical results in Figure 3, which is one of the pertinent results of our study. The two groups of points show a remarkable resemblance (with the exception of the layer separation of the 180-AB_4 structure, being predicted slightly too large), based on which we are the first to assign stacking labels—and thus detailed structural information—to the experimental results. This result suggests that the temperature at which the sample is prepared determines the stacking configuration that dominates the sample. It is important to mention that, although we find excellent agreement between experiment and theory concerning the change in the band gap as a function of layer distance, there is a discrepancy in the absolute values of the band gaps of ∼0.2 eV. This discrepancy is partly the result of vdW-DF's well-know

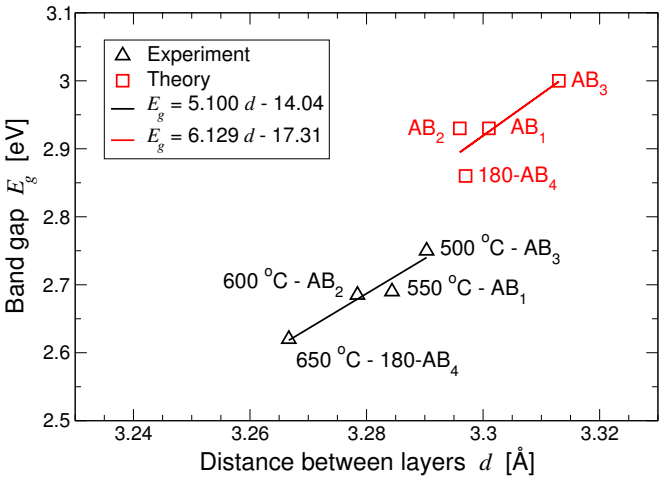

Fig. 3 Band gap E_g vs. separation of layers d. Linear fits have been included for both the experimental and theoretical results.

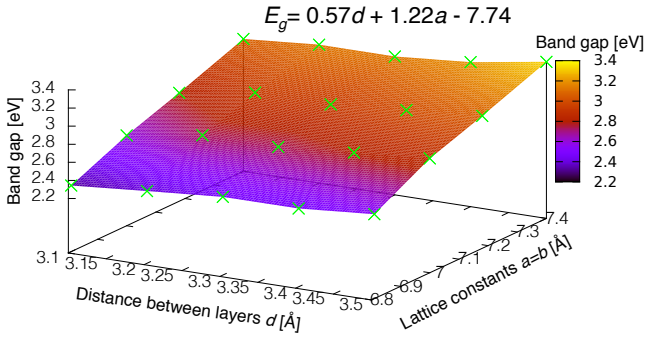

Fig. 4 Band gap vs. lattice constants for the g-C_3N_4 in the AB_1 stacking configuration. The green marks show the points for which we have calculated the band gap. In between this grid, the band gap is linearly interpolated.

tendency to overestimate lattice constants.[60] If we calculate the band gap for the experimental lattice constants of e.g. 180-AB_4 ($a = b = 6.81$ and $d = 3.267$ Å), we find a band gap of 2.73 eV, which is within 4% of the experimental value. Note that with the *GW* method we calculate the quasi-particle gap, while our experiments measure the optical gap, and their difference is related to the exciton binding energy. As such, the remainder of the discrepancy is likely due to excitonic effects, which Wei and co-workers have found to be important in related systems.[61]

The assignment of the dominating stacking configuration to the experimental data in Figure 3 is also supported by Figures S1 and S2 of the supplementary materials, where we analyze the peak in the XRD spectra around 45° further. Figure S2 of the supplementary materials shows that all of our calculated stacking configurations exhibit two peaks at 43.7° and 45.8° and that their heights gradually shift from the latter to the former with decreasing total energy. As the two peaks cannot be resolved separately in experiments, this manifests itself in a slight overall shift to lower angles of the broad peak measured, which is exactly what is observed experimentally in Figure S1 in the supplementary materials.

Although not the main focus of this paper, one interesting question remains—why do the samples assume different stacking configurations when prepared at different temperatures? We see from Table 1 and Figure 3 that increasing temperatures leads to lower-energy stackings. It is tempting to assume that the local energy minima of the higher-energy stacking configurations are "larger" (and thus easier to get trapped into) and that lower-energy stackings are separated by increasingly larger barriers that can only be overcome by sufficiently high temperatures. However, from our random-structure search we find that the first statement is not true. And, from nudged-elastic band calculations to find the transition states between stackings, we further find that the second statement is not true either—the energy barriers separating stackings are of such magnitude (on the order of 1 k_BT) that they can easily be overcome at room temperature. As such, further research is needed to answer this question and at the moment we are performing *ab initio* molecular-dynamics simulations to study the behavior of this system as a function of temperature.

3.2 A Model System

In the previous section we made the relationship between the layer separation and the band gap explicit, providing even a linear equation in Figure 3. However, we have not yet explained the physical origin of this peculiar relationship, which is the main focus of the present section. To this end, we use the stacking configuration AB_1 as a model system and analyze this relationship further. Note that we could have used either of the other stackings, with only minimal changes in the results.

First, we calculate the band gap of the system as a function of the lattice constants $a = b$ and the distance between layers d; results are presented in Figure 4. From this figure it is obvious that the relation is almost perfectly linear in both dimensions and we provide the equation of the corresponding fitted plane. To explain this behavior, in Figure 5 we plot the local density of states (LDOS) of the N atom at the edge of the tri-*s*-triazine unit for two different lattice constants. From the figure it can be seen that, in both cases, the top of the valence band is comprised of s, p_x, and p_y states, while the bottom of the conduction band is comprised only of unoccupied p_z states. In particular, we find that the unoccupied p_z states shift towards higher energies as the lattice constant a increases from 6.81 to 7.40 Å. In general, and true for all grid points calcu-

This journal is © The Royal Society of Chemistry [year]

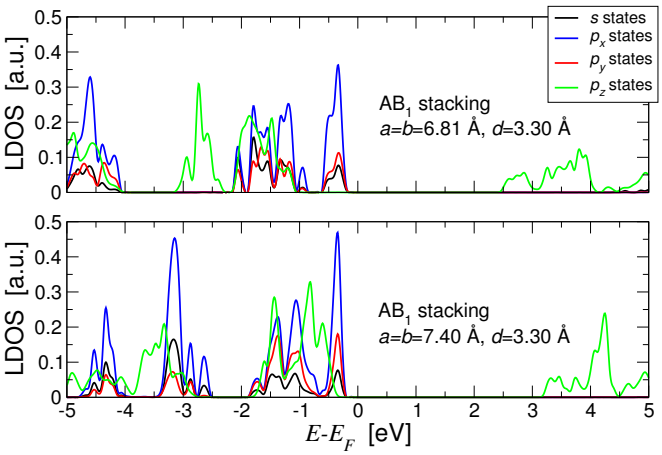

Fig. 5 LDOS of the N atom at the edge of the tri-*s*-triazine unit, resolved into the states s, p_x, p_y, and p_z. The upper and lower panel show the LDOS for different lattice constants.

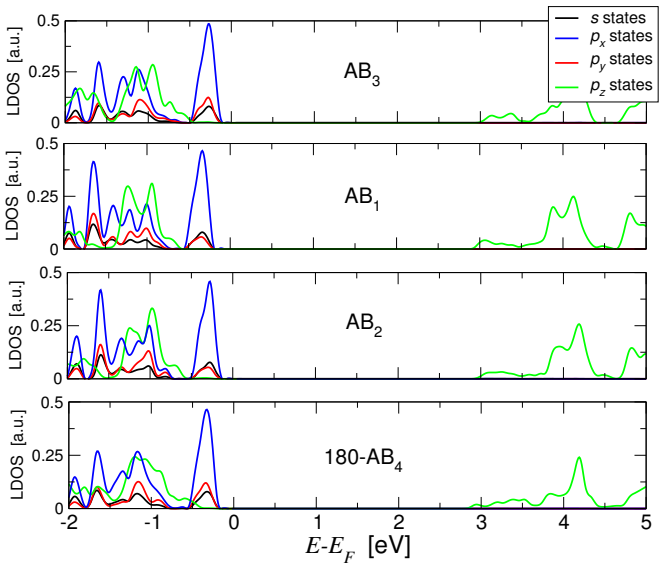

Fig. 6 LDOS of the N atom at the edge of the tri-*s*-triazine unit. The LDOS has been resolved into the states s, p_x, p_y and p_z.

lated in Figure 4, the p_z states experience a higher energy shift than the s, p_x, and p_y states, causing the band gap to increase as the lattice constant a increases. The exact same behavior is found for increasing the layer separation d.

This is a well-known effect also observed in other systems,[62] due to the reduction of hybridization between p_z states of neighboring atoms, and we identify it here as the main mechanism underlying the structure/band gap relationship in g-C_3N_4. To further support this conclusion, we again use the AB$_1$ model system and calculate its band gap as the two layers are rigidly slid agains each other from 0 to 0.6 Å along the unit vector b. This way, the hybridization between atoms of adjacent layers is forced to gradually grow. Indeed, we find that the conduction band of the system is gradually displaced towards lower energies and the band gap continuously changes from 2.93 to 2.88 eV. In summary, the hybridization and overlap of the p_z states, which clearly depends on structural aspects such as the lattice constants, is the determining mechanism in the structure/band gap relationship.

We conclude this section by estimating pressures necessary to lower the band gap of g-C_3N_4. As can be seen in Figure 4, the largest effect would result from reducing the lattice constants a and b—but this is technologically not feasible, in particular in a powder. On the other hand, from the same figure we know also the change in the band gap with layer separation d, and we also know the total energy as a function of d. As such, we can calculate the pressure required to reach a particular layer separation and can then relate this to the band gap, as can be seen in Figure S3 of the supplementary materials. Overall, we find that fairly large pressures are required and the band gap changes by 0.03 eV for every GPa of pressure along the c-axis. On the other hand, it may be possible to change the in-plane lattice constant of g-C_3N_4 by growing it on a lattice-mismatch substrate such as graphite, boron nitride, or metals with hexagonal structures. Of particular promise is Sc, which exhibits the necessary hexagonal symmetry with a lattice constant of 3.31 Å when cleaved along the [0001] plane, potentially resulting in a band gap of 2.51 eV (according to our fit from Figure 3).

3.3 Generalization to g-C_3N_4

In the previous section we found that the hybridization of p_z states is responsible for the almost linear relationship between the lattice constants and band gap in the model AB$_1$ system. However, these results are easily generalized to the other stackings and in Figure 6 we plot the LDOS of the N atom at the edge of the tri-*s*-triazine unit for the various stackings considered. As expected, the conduction band in all four systems is comprised only of p_z states and the band gap is governed by the position of these states. In all cases the band gap is susceptible to stress and to the stacking configuration adopted by the system through the same mechanism, i.e. the conduction band of all stackings experiences large variations, while the valence band experiences only small shifts upon changes in the geometry of the system.

This mechanism also explains the findings of Li et al.,[44] where oxygen doping was found to decrease the band gap of g-C_3N_4 by 0.21 eV. We now know that the influence of oxygen upon the electronic structure and thus the band gap is mostly indirect, in that it changes the layer separation from 3.26 Å to 3.24 Å and thus indirectly influences the band gap through our proposed mechanism. This opens the door for a different line

of research, where the main focus is on decreasing the layer separation by means of doping or intercalating g-C_3N_4—a direction we are already actively pursuing.

4 Summary

In this work we combine experimental spectroscopy and *ab initio* calculations to study the g-C_3N_4 system. We have shown that the band gap of g-C_3N_4 depends on the stacking configuration and, more generally, it depends on the lattice constants in an almost perfectly linear relationship. We explain this peculiar finding by analyzing the density of states and find that the top of the valence band in this system is comprised of s, p_x, and p_y states, while the bottom of the conduction band is comprised of p_z states only. As the lattice constants decrease, the increase of overlap between p_z states of neighboring atoms causes them to experience a higher energy shift than the s, p_x, and p_y states. As a consequence, the band gap shrinks.

Our main finding is the uncovering of this underlying mechanism that controls the structure/band gap relationship. Knowledge and understanding of this mechanism is essential for further band-gap tuning of g-C_3N_4 for the purpose of photocatalysis, where it controls the frequency of light absorbed and thus the efficiency of such devices. Our main point is that band-gap tuning should focus on decreasing the lattice constants of this system. Although we show that this is possible through high external pressure, we believe that doping, intercalating, or stress created by lattice mismatch is the most promising way to tune the band gap of g-C_3N_4.

Acknowledgements

This work was supported by Department of Energy Grant No. DE-FG02-08ER46491. NS, who performed the XRD measurements, was supported by DOE grant No. de-sc0010697. The authors would also like to thank Dr. Weina Peng from the Department of Materials Science and Engineering, University of Texas at Dallas, for her valuable discussions.

References

1 L. Barreto, A. Makihira and K. Riahi, *Int. J. Hydrogen Energy*, 2003, **28**, 267–284.
2 M. Conte, A. Iacobazzi, M. Ronchetti and R. Vellone, *J. Power Sources*, 2001, **100**, 171–187.
3 S. Penner, *Energy*, 2006, **31**, 33–43.
4 G. Marbán and T. Valdés-Solís, *Int. J. Hydrogen Energy*, 2007, **32**, 1625–1637.
5 A. L. Linsebigler, G. Lu and J. T. Yates, *Chem. Rev.*, 1995, **95**, 735–758.
6 A. Fujishima, T. N. Rao and D. A. Tryk, *J. Photochem. Photobiol. C*, 2000, **1**, 1–21.
7 M. A. Fox and M. T. Dulay, *Chem. Rev.*, 1993, **93**, 341–357.
8 A. Mills and S. L. Hunte, *J. Photochem. Photobiol. A*, 1997, **108**, 1–35.
9 M. Ni, M. K. H. Leung, D. Y. C. Leung and K. Sumathy, *Renew. Sustain. Energy Rev.*, 2007, **11**, 401–425.
10 Q. Li, B. Guo, J. Yu, J. Ran, B. Zhang, H. Yan and J. R. Gong, *J. Am. Chem. Soc.*, 2011, **133**, 10878–10884.
11 H. Yan, J. Yang, G. Ma, G. Wu, X. Zong, Z. Lei, J. Shi and C. Li, *J. Catal.*, 2009, **266**, 165–168.
12 Z. Zou, J. Ye, K. Sayama and H. Arakawa, *Nature*, 2001, **414**, 625–627.
13 T.-F. Yeh, J.-M. Syu, C. Cheng, T.-H. Chang and H. Teng, *Adv. Funct. Mater.*, 2010, **20**, 2255–2262.
14 X. Zong, H. Yan, G. Wu, G. Ma, F. Wen, L. Wang and C. Li, *J. Am. Chem. Soc.*, 2008, **130**, 7176–7177.
15 N. Serpone, *J. Phys. Chem. B*, 2006, **110**, 24287–24293.
16 T. Morikawa, R. Asahi, T. Ohwaki, K. Aoki and Y. Taga, *Jpn. J. Appl. Phys.*, 2001, **40**, L561.
17 K. Nagaveni, M. S. Hegde, N. Ravishankar, G. N. Subbanna and G. Madras, *Langmuir*, 2004, **20**, 2900–2907.
18 X. H. Wang, J.-G. Li, H. Kamiyama, M. Katada, N. Ohashi, Y. Moriyoshi and T. Ishigaki, *J. Am. Chem. Soc.*, 2005, **127**, 10982–10990.
19 W. Zhu, X. Qiu, V. Iancu, X.-Q. Chen, H. Pan, W. Wang, N. M. Dimitrijevic, T. Rajh, H. M. Meyer, M. P. Paranthaman, G. M. Stocks, H. H. Weitering, B. Gu, G. Eres and Z. Zhang, *Phys. Rev. Lett.*, 2009, **103**, 226401.
20 W.-J. Yin, S. Chen, J.-H. Yang, X.-G. Gong, Y. Yan and S.-H. Wei, *Appl. Phys. Lett.*, 2010, **96**, 221901.
21 W.-J. Ong, L.-L. Tan, S.-P. Chai, S.-T. Yong and A. R. Mohamed, *Nano Research*, 2014, **7**, 1528–1547.
22 X. Qian, K. Fuku, Y. Kuwahara, T. Kamegawa, K. Mori and H. Yamashita, *ChemSusChem*, 2014, **7**, 1528–1536.
23 Y. Xing, W. Que, X. Liu, H. M. A. Javed, Z. He, Y. He and T. Zhou, *RSC Advances*, 2014, **4**, 49900–49907.
24 C. Xu, G. P. Rangaiah and X. S. Zhao, *Ind. Eng. Chem. Res.*, 2014, **53**, 14641–14649.
25 G. D. Moon, J. B. Joo, I. Lee and Y. Yin, *Nanoscale*, 2014, **6**, 12002–12008.
26 A. Thomas, A. Fischer, F. Goettmann, M. Antonietti, J.-O. Müller, R. Schlögl and J. M. Carlsson, *J. Mater. Chem.*, 2008, **18**, 4893–4908.
27 Y. Xu and S.-P. Gao, *Int. J. Hydrogen Energy*, 2012, **37**, 11072–11080.
28 F. Dong, L. Wu, Y. Sun, M. Fu, Z. Wu and S. C. Lee, *J. Mater. Chem.*, 2011, **21**, 15171–15174.
29 S. C. Yan, Z. S. Li and Z. G. Zou, *Langmuir*, 2009, **25**, 10397–10401.
30 S. C. Yan, Z. S. Li and Z. G. Zou, *Langmuir*, 2010, **26**, 3894–3901.
31 Y. Min, X. F. Qi, Q. Xu and Y. Chen, *CrystEngComm*, 2014, **16**, 1287–1295.
32 J. Yu, K. Wang, W. Xiao and B. Cheng, *Phys. Chem. Chem. Phys.*, 2014, **16**, 11492–11501.
33 K.-i. Katsumata, R. Motoyoshi, N. Matsushita and K. Okada, *J. Hazard. Mater.*, 2013, **260**, 475 – 482.
34 K. Maeda, K. Sekizawa and O. Ishitani, *Chem. Commun.*, 2013, **49**, 10127–10129.
35 H. Shi, G. Chen, C. Zhang and Z. Zou, *ACS Catal.*, 2014, **4**, 3637–3643.
36 J. Ran, J. Zhang, J. Yu, M. Jaroniec and S. Z. Qiao, *Chem. Soc. Rev.*, 2014, **43**, 7787–7812.
37 A. B. Jorge, D. J. Martin, M. T. S. Dhanoa, A. S. Rahman, N. Makwana, J. Tang, A. Sella, F. Corà, S. Firth, J. A. Darr and P. F. McMillan, *J. Phys. Chem. C*, 2013, **117**, 7178–7185.
38 X. Wang, K. Maeda, A. Thomas, K. Takanabe, G. Xin, J. M. Carlsson, K. Domen and M. Antonietti, *Nat. Mater.*, 2009, **8**, 76–80.
39 J. Liu, T. Zhang, Z. Wang, G. Dawson and W. Chen, *J. Mater. Chem.*, 2011, **21**, 14398–14401.
40 G. Liu, P. Niu, C. Sun, S. C. Smith, Z. Chen, G. Q. M. Lu and H.-M. Cheng, *J. Am. Chem. Soc.*, 2010, **132**, 11642–11648.

This journal is © The Royal Society of Chemistry [year]

41 J. Zhang, J. Sun, K. Maeda, K. Domen, P. Liu, M. Antonietti, X. Fu and X. Wang, *Energy Environ. Sci.*, 2011, **4**, 675–678.

42 Y. Zhang, T. Mori, J. Ye and M. Antonietti, *J. Am. Chem. Soc.*, 2010, **132**, 6294–6295.

43 G. Dong, K. Zhao and L. Zhang, *Chem. Commun.*, 2012, **48**, 6178–6180.

44 J. Li, B. Shen, Z. Hong, B. Lin, B. Gao and Y. Chen, *Chem. Commun.*, 2012, **48**, 12017–12019.

45 B. Yue, Q. Li, H. Iwai, T. Kako and J. Ye, *Sci. Technol. Adv. Mater.*, 2011, **12**, 034401.

46 Y. Wang, J. Zhang, X. Wang, M. Antonietti and H. Li, *Angew. Chem., Int. Ed.*, 2010, **49**, 3356–3359.

47 L. Yang, M. P. Anantram, J. Han and J. P. Lu, *Phys. Rev. B*, 1999, **60**, 13874–13878.

48 Z. H. Ni, T. Yu, Y. H. Lu, Y. Y. Wang, Y. P. Feng and Z. X. Shen, *ACS Nano*, 2008, **2**, 2301–2305.

49 E. D. Minot, Y. Yaish, V. Sazonova, J.-Y. Park, M. Brink and P. L. McEuen, *Phys. Rev. Lett.*, 2003, **90**, 156401.

50 L. Sun, Q. Li, H. Ren, H. Su, Q. W. Shi and J. Yang, *J. Chem. Phys.*, 2008, **129**, 074704.

51 H. H. Pu, S. H. Rhim, C. J. Hirschmugl, M. Gajdardziska-Josifovska, M. Weinert and J. H. Chen, *Phys. Rev. B*, 2013, **87**, 085417.

52 G. Kresse and J. Furthmüller, *Phys. Rev. B*, 1996, **54**, 11169–11186.

53 G. Kresse and D. Joubert, *Phys. Rev. B*, 1999, **59**, 1758–1775.

54 M. Dion, H. Rydberg, E. Schröder, D. C. Langreth and B. I. Lundqvist, *Phys. Rev. Lett.*, 2004, **92**, 246401.

55 T. Thonhauser, V. R. Cooper, S. Li, A. Puzder, P. Hyldgaard and D. C. Langreth, *Phys. Rev. B*, 2007, **76**, 125112.

56 D. C. Langreth, B. I. Lundqvist, S. D. Chakarova-Käck, V. R. Cooper, M. Dion, P. Hyldgaard, A. Kelkkanen, J. Kleis, L. Kong, S. Li, P. G. Moses, E. D. Murray, A. Puzder, H. Rydberg, E. Schröder and T. Thonhauser, *J. Phys. Condens. Matter*, 2009, **21**, 084203.

57 L. Hedin, *Phys. Rev.*, 1965, **139**, A796–A823.

58 S. Stolbov and S. Zuluaga, *J. Phys.: Condens. Matter*, 2013, **25**, 085507.

59 M. J. Bojdys, J.-O. Müller, M. Antonietti and A. Thomas, *Chem. - Eur. J.*, 2008, **14**, 8177–8182.

60 T. Thonhauser, A. Puzder and D. C. Langreth, *J. Chem. Phys.*, 2006, **124**, 164106.

61 W. Wei and T. Jacob, *Phys. Rev. B*, 2013, **87**, 085202.

62 S. Stolbov and S. Zuluaga, *J. Phys. Chem. Lett.*, 2013, **4**, 1537–1540.

Structural band-gap tuning in g-C_3N_4
— Supplementary Materials —

Sebastian Zuluaga,[1] Li-Hong Liu,[2] Natis Shafiq,[2] Sara Rupich,[2]
Jean-François Veyan,[2] Yves J. Chabal,[2] and Timo Thonhauser[1]

[1] *Department of Physics, Wake Forest University, Winston-Salem, North Carolina 27109, USA*
[2] *Department of Materials Science and Engineering, University of Texas at Dallas, Dallas, Texas 75080, USA*

(Dated: December 12, 2014)

arXiv:1412.3485v1 [cond-mat.mtrl-sci] 10 Dec 2014

I. ULTRAVIOLET PHOTOELECTRON SPECTROSCOPY

Ultraviolet photoelectron spectroscopies (UPS) were obtained on a PHI Versa Probe II scanning XPS microprobe, Physical Electronics, equipped with a Prevac UV source (UV40A). The UPS radiation is generated by a He-gas discharge lamp (He I = 21.22 eV; UV source settings: $I_{\text{emis}} = 100$ mA, $U_{\text{source}} = 0.52$ kV, $P_{\text{He}} = 9.6 \times 10^{-2}$ mbar), and measurements were made using the He I excitation (21.2 eV) and recorded with a constant pass energy of 1.75 eV in the ultrahigh vacuum chamber of the XPS instrument. Samples were placed at normal incidence to the analyzer. The source to analyzer angle was set to 45°. During the measurement, both e-gun and Ar gun were turned on for neutralization. The pressure in the main chamber was 2.6×10^{-7} Pa. Samples were loaded in the UHV chamber overnight to allow sample degasing and to let the UHV pressure drop below 1×10^{-6} Pa.

Figure S4 shows a series of UPS spectra for the four g-C_3N_4 samples prepared at 500, 550, 600, and 650 °C in the valence band region. In particular, the E_{VB} positions, based on linear extrapolation, are shown and numerical values are collected in Table S1. Because the samples are insulators at room temperature, their work function cannot be measured by standard bias techniques using UPS.

TABLE S1. Band gap, E_g, and the positions of the valence and conduction bands, E_{VB} and E_{CB}, in eV with respect to the Fermi level for the four g-C_3N_4 samples prepared at different temperatures.

Temperature	E_g	E_{VB}	E_{CB}
500 °C	2.75	−0.90	1.85
550 °C	2.69	−0.90	1.79
600 °C	2.68	−0.90	1.78
650 °C	2.62	−1.13	1.49

II. FIGURES

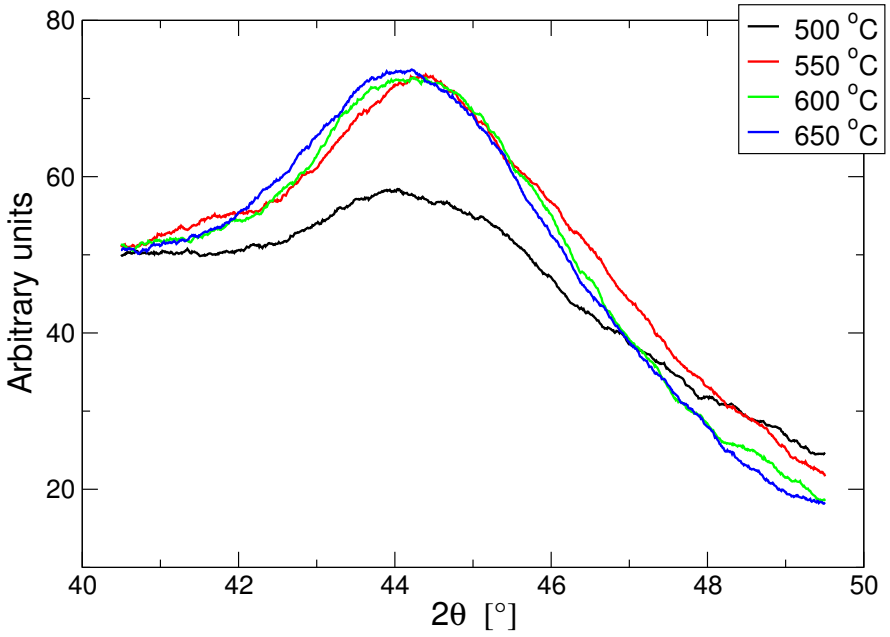

FIG. S1. Enlarged experimental XRD spectra around the peak at $\sim 45°$ for the g-C_3N_4 samples prepared at 500, 550, 600, and 650 °C.

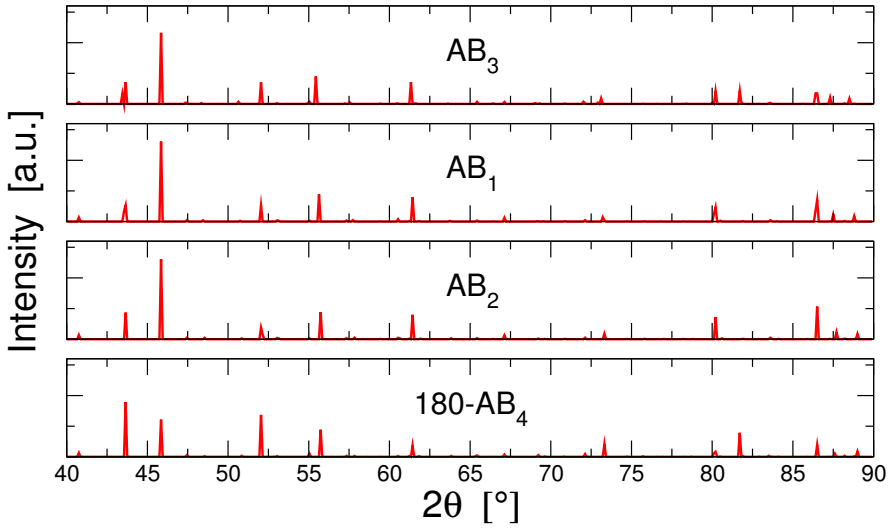

FIG. S2. Calculated XRD spectra at higher angles for the four g-C_3N_4 stacking configurations.

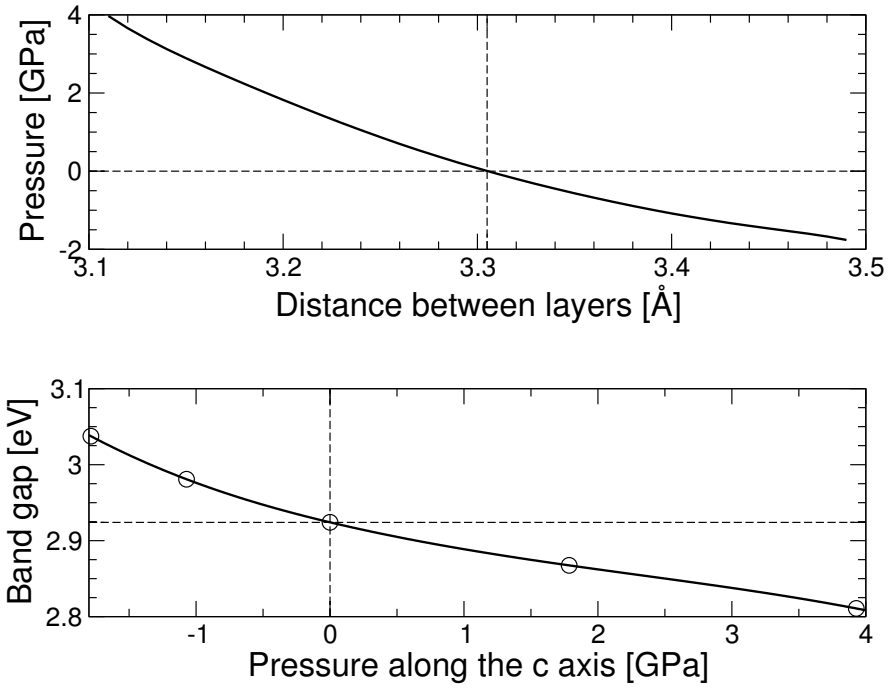

FIG. S3. (top) Pressure vs. layer separation d in the AB_1 stacking of g-C_3N_4. (bottom) Band gap of AB_1 as a function of the applied pressure along the c axis.

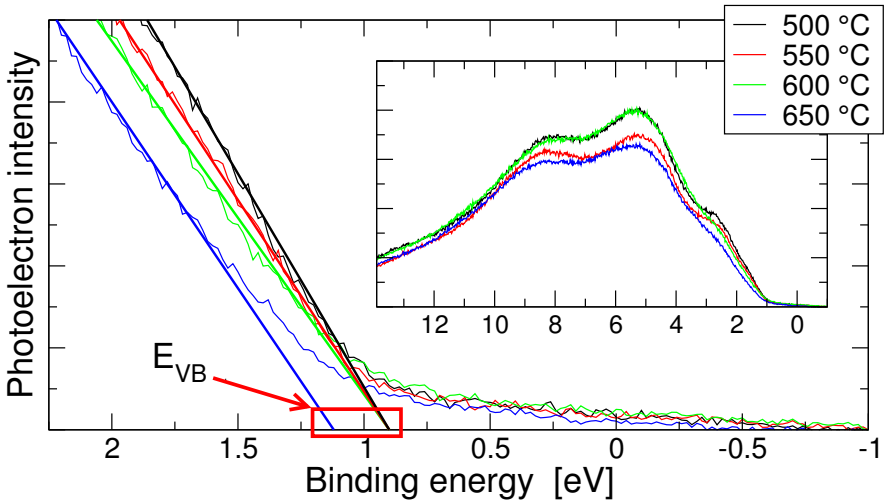

FIG. S4. UPS spectra in the valence band region of the four g-C_3N_4 samples prepared at 500, 550, 600, and 650 °C. The inset shows the full spectra between −1 and 13 eV.